

Simulation Study on a New Hybrid Autonomous Underwater Vehicle with Elevators

Jiafeng Huang^{1,2}, Hyeung-Sik Choi^{1,*}, Dong-Wook Jung^{1,2}, Hyunjoon Cho¹, Phan Huy Nam Anh^{1,2},
Ruo Chen Zhang^{1,2}, Jung-Hyeun Park^{1,2}, Chi-Ung Yun^{1,2}

¹Department of Mechanical Engineering; ²Interdisciplinary Major of Ocean Renewable Energy Engineering, Korea Maritime & Ocean University, Busan, Korea

Received 08 June 2023 received in revised form 18 August 2023; accepted 19 August 2023

DOI: <https://doi.org/10.46604/peti.2023.12343>

Abstract

This study aims to design a new hybrid twin autonomous underwater vehicle (HTAUV) consisting of dual cylinder hulls and analyze its pitching motion. The kinematic model for the HTAUV is established, followed by the execution of hydrodynamic simulation CFD of the HTAUV using Ansys Fluent. These simulations are conducted to obtain the hydrodynamic force equation of the HTAUV, which relates to the deflection angle of the elevator. Through the motion simulation of the HTAUV, under the same net buoyancy condition, notable differences emerge when the elevator is deflected. Specifically, parameters such as gliding speed, gliding angle, and pitch angle of the HTAUV are larger when the elevator is deflected, as compared to cases where no deflection is applied.

Keywords: HTAUV, hydrodynamic parameters, elevator, CFD simulation

1. Introduction

Underwater robots play an important role in the exploration of the unknown underwater world [1], which are remotely operated vehicles (ROVs), autonomous underwater vehicles (AUVs), and underwater gliders (UGs) represent underwater robots. ROVs are operated by a human operator using a remote control, and they are tethered to a surface vessel, which supplies power and communications. ROVs can be used for deep-sea exploration, search and rescue operations, and underwater construction and maintenance [2]. AUVs are self-propelled and operate without human intervention, AUVs are used for mapping the ocean floor, oceanography, and marine biology research [3]. UGs move through the water by changing their buoyancy. They use a low-power propulsion system to navigate and are used for long-term ocean monitoring [4]. However, the operational duration of AUVs are not long and the UGs' motion is sinusoidal such that they can not inspect or monitor underwater surface. To solve this problem, a study on a new underwater vehicle is required.

A hybrid twin autonomous underwater vehicle (HTAUV) is a type of underwater robot that is designed to have the hybrid functions of the AUV and the UG. It combines two different propulsion systems, typically a gliding system (UG mode) and a propeller or thruster system (AUV mode), to provide long-range movement and accurate inspection on the underwater surface. The twin configuration of the body provides increased stability and maneuverability [5], allowing it to navigate through complex underwater environments with ease, making it an ideal platform for a variety of oceanographic applications, including scientific research, environmental monitoring, and underwater mapping [6]. Based on the uncertainty of the underwater environment and the limitations of the system, there are certain challenges and difficulties in the control of AUVs [7]. Computer fluid dynamic (CFD) simulation is one of the most common ways to obtain hydrodynamic parameters of underwater

* Corresponding author. E-mail address: hchoi@kmou.ac.kr

equipment easily and quickly in the research process of underwater equipment [8-12]. Nguyen et al. [13] have proposed a robust adaptive control algorithm for the hybrid underwater glider (HUG). In the descend and ascend periods, the pitch control is designed using the backstepping technique and direct adaptive control. A new method of detecting the position of the docking station using a light source is presented. Also, a newly developed optical sensor which makes it much easier to sense the light source than the camera system for homing of the AUV under the water is performed [14].

In the HTAUV, the pitching motion is very important for accurate underwater inspection, which is controlled by the elevator. The main purpose of this paper is to analyze and study the effect of the elevator on the motion of HTAUV in the vertical plane. In this paper, Ansys Fluent is used to simulate the hydrodynamic force of THAUV under different elevator deflection angles to obtain the relationship between hydrodynamic lift, drag, hydrodynamic moment, and elevator deflection angle. Through the simulation results, the direction of the deflection angle of the elevator during the diving and surfacing of the THAUV can be obtained.

2. Design of the HTAUV and Mathematic Model

As a platform for underwater monitoring and detection, the HTAUV consists of a combination of multiple components that are considered individual rigid bodies, and the kinematic equations of the HTAUV are obtained by analyzing the motions of these rigid bodies. This section focuses on the structural design of the HTAUV and the construction of the kinematic model of the HTAUV.

2.1. Structure of the HTAUV

The HTAUV is a new type of underwater monitoring platform with two buoyant bodies, which allows it to carry more energy and a variety of measurement equipment. The two buoyant bodies are connected by an aluminum plate, which can also be considered as a fixed-wing of the HTAUV. The size of the fixed wing plate not only determines the hydrodynamic lift, drag, and hydrodynamic moment received by the HTAUV during underwater operation but also the stability of the overall HTAUV structure. Most of the hydrodynamic resistance to HTAUV operation underwater comes from the viscous forces on the buoyant body. To reduce the resistance to underwater movement, the main body of the HTAUV is a torpedo-shaped rotating body, the rotating body is modeled using the Myring hull profile equations. The structure of the HTAUV is illustrated in Fig. 1.

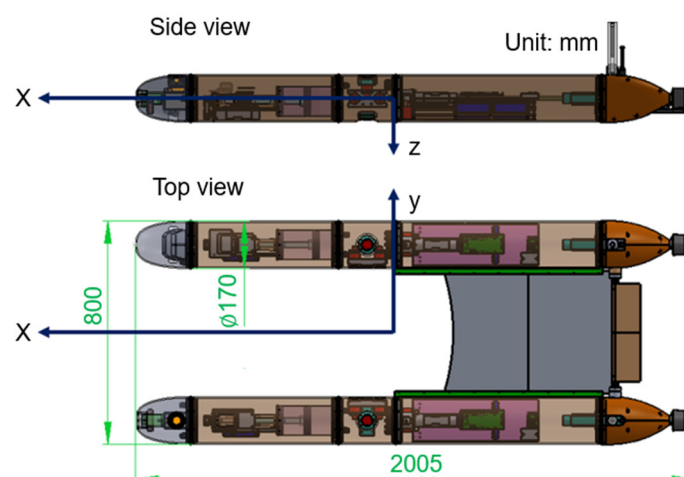


Fig. 1 The structure of HTAUV

The HTAUV is a comprehensive electronics platform that is equipped with a control system, sensors, and electronic devices inside the hull. The sensors are the camera, Doppler velocity logger (DVL), altimeter, ultra-short baseline (USBL), conductivity, temperature, depth (CTD), antenna, image sonar, and optical communication system. Fig. 2 depicts the detailed equipment layout of the HTAUV.

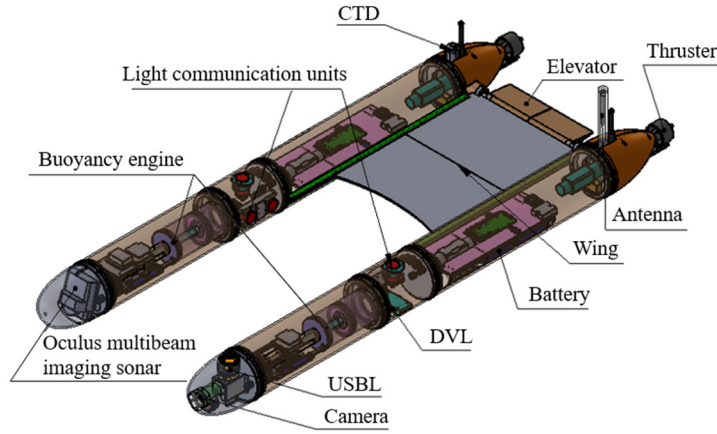


Fig. 2 The detailed equipment layout of HTAUV

An aluminum plate wing is attached between the two buoyant bodies. This arrangement ensures not only the structural stability of the HTAUV during underwater navigation but also provides a hydrodynamic lift for the HTAUV during ascents and descents. As a result, the HTAUV can achieve a gliding mode without the need for power. As shown in Fig. 1, the HTAUV is approximately symmetric about the xz -plane in the top view and about the xy -plane in the side view. A pair of elevators are installed at the rear of the fuselage, mainly to control the hydrodynamic moment generated by the HTAUV while sailing underwater and to achieve pitch attitude control.

HTAUV is an underwater vehicle where the change in buoyancy force, generated by the buoyancy engine, facilitates the sinking and floating of HTAUV in the water. During the sinking and surfacing motion of HTAUV, the fixed airfoil experiences a reaction force from the surrounding fluid that propels it forward, resulting in a cyclic zigzag motion trajectory. The design in this paper uses a piston-cylinder type buoyancy engine mechanism, which achieves periodic changes in buoyancy through the reciprocating motion of the piston. The piston, piston rod, and other parts constitute an integral unit within the HTAUV, and their position is adjustable.

Therefore, the piston assembly can be considered a movable mass. To achieve imaging scanning of submarine slopes with slope, roll control of HTAUV is achieved in this design utilizing motor-driven roller masses. Additionally, a roller deflection system is configured in both buoyant bodies. Since the deflection angle of the elevator is small and the center of mass of the elevator is located close to the XY plane of HTAUV's body coordinate system, the changes in the center of mass and floating center caused by the deflection of the elevator are ignored in this paper. The distribution of mass points and center of mass in HTAUV is shown in Fig. 3.

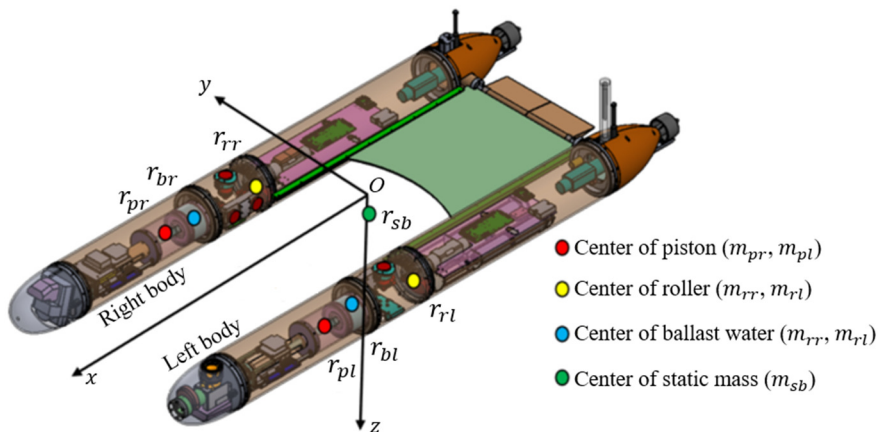


Fig. 3 The distribution of mass points and center of mass

HTAUV is a rigid body system consisting of a piston assembly ($m_{pr} + m_{pl}$), a rotating mass ($m_{rr} + m_{rl}$) and a static mass (m_{sb}). In this paper, the effect of the rotating masses is not considered and their positional coordinates are always constant,

then the static mass in this case is m_s ($m_{rr} + m_{rl} + m_{sb}$). To avoid the unstable operation of the left and right sides due to the buoyancy difference, the pistons of the left and right buoyancy engines will be synchronized, and thus the pistons on both sides are considered as one mass block (m_p). The total mass of HTAUV consists of several components, and the total mass equation can be expressed by:

$$m = m_{pr} + m_{pl} + m_{rr} + m_{rl} + m_{sb} = m_p + m_s \quad (1)$$

The position of the center of mass of each mass is shown in Fig. 3, and the center of mass of HTAUV can be obtained by extrapolating the following equation

$$\mathbf{r}_{CG} = [m_{pr}\mathbf{r}_{pr} + m_{pl}\mathbf{r}_{pl} + m_{rr}\mathbf{r}_{rr} + m_{rl}\mathbf{r}_{rl} + m_{sb}\mathbf{r}_{sb}]/m \quad (2)$$

\mathbf{r}_{pr} , \mathbf{r}_{pl} , \mathbf{r}_{rr} , \mathbf{r}_{rl} , and \mathbf{r}_{sb} in Eq. (2) are the positional coordinates of the pistons on the left and right sides, the rotating rollers on both sides and the static mass of the body in the body coordinate system, respectively.

The HTAUV uses a piston-type buoyancy engine to change the buoyancy force underwater. When the piston sucks in water, the buoyancy force is less than gravity, and the HTAUV moves downward. When the piston drains the water, the resulting buoyancy force is greater than gravity, causing the HTAUV to move upward. To avoid the instability of the HTAUV caused by the difference in buoyancy between the left and right sides, both sides of the buoyancy engine will work in synchronization. The left and right sides of the buoyancy engine have equal ballast water and the equation for the ballast water can be expressed by:

$$m_b = \rho\pi r^2 d_p = u_0 d_p \quad (3)$$

Here, ρ is the density of water, r is the radius of the piston ($r = 0.05m$), and d_p is the displacement of the piston along the x-axis. In the initial state, the HTAUV is suspended in water, achieving equilibrium between gravity and buoyancy. The net buoyant mass of the HTAUV is the mass of ballast water in the two buoyancy engines. Therefore, the expression of the net buoyancy of HTAUV can be expressed by:

$$m_0 = 2 \times m_b \quad (4)$$

This paper focuses on the effect of the tail-end elevator on the pitch angle of the HTAUV in the vertical plane. When the HTAUV reaches a stable glide underwater, the forces on it will reach an equilibrium state, and the force schematic of the HTAUV is shown in Fig. 4. The symbols of each parameter in Fig. 4 are explained as follows: θ , α , and ζ represent the pitch angle, angle of attack, and glide angle of the HTAUV, respectively. L , D , and M_{DL} are the hydrodynamic lift, drag, and hydrodynamic moment on the HTAUV, respectively.

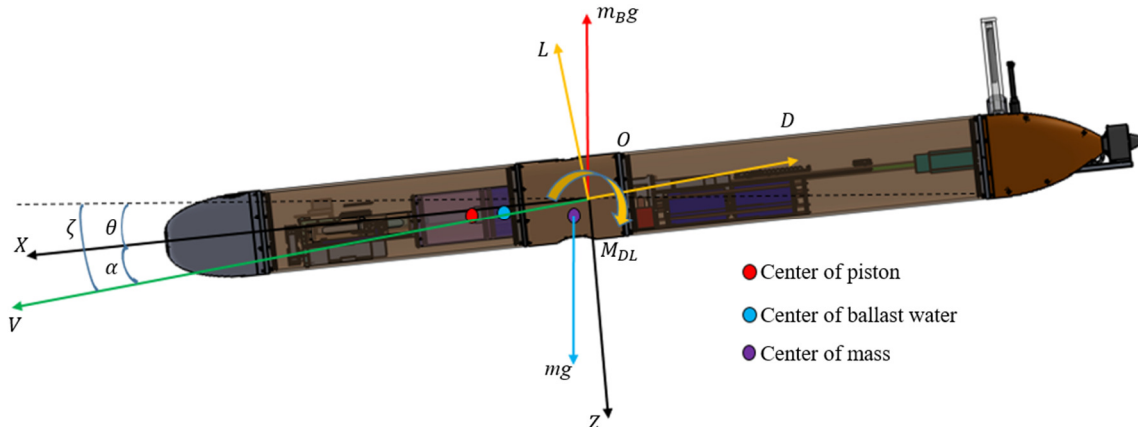


Fig. 4 The forces schematic of the HTAUV

2.2. Mathematic model of HTAUV

The coordinate system of HTAUV's motion was established, as shown in Fig. 5. The coordinate system includes a reference coordinate system E-XYZ, body coordinate system O-xyz with the buoyancy center of HTAUV as the coordinate origin, in addition to the velocity coordinate system π_0 of HTAUV's motion.

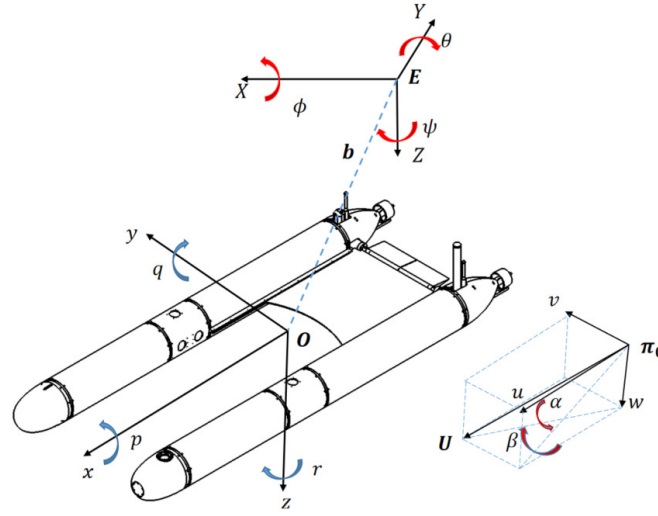


Fig. 5 The coordinates of the HTAUV

The size of the elevator is very tiny compared to the HTAUV body, and the amplitude of the deflection angle of the elevator is very small. Therefore, the effect of the elevator on the buoyancy and the added mass of the HTAUV during the deflection process is ignored in this paper, and only the effect of the deflection of the elevator on the hydrodynamic parameters is considered. As shown in Fig. 5, the position of HTAUV in the reference coordinate system can be expressed as the vector $\mathbf{b} = (x, y, z)^T$. The translational linear and angular velocities of HTAUV in the reference coordinate system are denoted as vectors $\mathbf{v} = (u, v, w)^T$ and $\boldsymbol{\omega} = (p, q, r)^T$, respectively.

In [15-16], detailed motion control equations for the underwater glider in three-dimensional space were derived. The orientation of the HTAUV relative to the conference coordinate system is specified by the rotation matrix R , which is expressed with three rotation angles (ϕ, θ, φ) . The transformation matrix from the body-fixed frame O-xyz to the conference coordinate E-XYZ can be expressed by:

$$R = \begin{bmatrix} \cos\psi\cos\theta & -\sin\psi\cos\phi + \cos\psi\sin\theta\sin\phi & \sin\psi\sin\phi + \cos\psi\cos\phi\sin\theta \\ \sin\psi\cos\theta & \cos\psi\cos\phi + \sin\psi\sin\theta\sin\phi & -\cos\psi\sin\phi + \sin\theta\sin\psi\cos\phi \\ -\sin\theta & \cos\theta\sin\phi & \cos\theta\cos\phi \end{bmatrix} \quad (5)$$

For a vector $\mathbf{x} = (x_1, x_2, x_3)^T$, the skew-symmetric matrix is expressed as:

$$\hat{\mathbf{x}} = \begin{bmatrix} \mathbf{0} & -x_3 & x_2 \\ x_3 & \mathbf{0} & -x_1 \\ -x_2 & x_1 & \mathbf{0} \end{bmatrix} \quad (6)$$

For any vector $\mathbf{y} = (y_1, y_2, y_3)^T$, the vector product of \mathbf{x} and \mathbf{y} is expressed as:

$$\hat{\mathbf{x}}\mathbf{y} = \mathbf{x} \times \mathbf{y} \quad (7)$$

The kinematics of the HTAUV can be written as:

$$\dot{R} = R\hat{\boldsymbol{\omega}} \quad (8)$$

$$\dot{\mathbf{b}} = R\mathbf{v} \quad (9)$$

Let \mathbf{P}_E and $\boldsymbol{\pi}_E$ represent the total linear momentum and angular momentum of the HTAUV in the Earth-fixed reference coordinate, respectively. $\mathbf{P}_{p,E}$ is denoted as the total momentum of the piston.

$$\dot{\mathbf{P}}_E = \sum_{i=1}^I \mathbf{f}_{ext,i} \quad (10)$$

$$\dot{\boldsymbol{\pi}}_E = \sum_{i=1}^I (\mathbf{x}_i \times \mathbf{f}_{ext,i}) + \sum_{j=1}^J \boldsymbol{\tau}_{ext,j} \quad (11)$$

$$\dot{\mathbf{P}}_{p,E} = m_p \mathbf{g} \mathbf{k} + \sum_{k=1}^K \mathbf{f}_{int,m_p} \quad (12)$$

Here, \mathbf{k} is a unit vector point in the direction of gravity, $\mathbf{f}_{ext,i}$ is the external force exerted on the glider system, and $\boldsymbol{\tau}_{ext,j}$ is the external torque applied to the system. Vector \mathbf{x}_i applies the point of application of the external force concerning the Earth's reference frame. The force \mathbf{f}_{int,m_p} exerts on the left and right pistons from the glider body.

\mathbf{P} represents the total linear momentum of the glider-fluid system expressed in the body-fixed reference frame, $\boldsymbol{\Pi}$ represents the total angular momentum of the origin of the body coordinate, and \mathbf{P}_p represents the total momentum of the left and right pistons.

$$\mathbf{P}_E = \mathbf{R}\mathbf{P} \quad (13)$$

$$\boldsymbol{\pi}_E = \mathbf{R}\boldsymbol{\Pi} + \mathbf{b} \times \mathbf{P}_E \quad (14)$$

$$\mathbf{P}_{p,E} = \mathbf{R}\mathbf{P}_p \quad (15)$$

Combining Eqs. (8) and (9), the derivatives on both sides of Eqs. (10)-(15) above can be calculated as follows:

$$\dot{\mathbf{P}}_E = \mathbf{R}(\dot{\mathbf{P}} + \hat{\boldsymbol{\omega}}\mathbf{P}) \quad (16)$$

$$\dot{\boldsymbol{\pi}}_E = \mathbf{R}(\dot{\boldsymbol{\Pi}} + \hat{\boldsymbol{\omega}}\boldsymbol{\Pi}) + \mathbf{R}\mathbf{v} \times \mathbf{P}_E + \mathbf{b} \times \dot{\mathbf{P}}_E \quad (17)$$

$$\dot{\mathbf{P}}_{p,E} = \mathbf{R}(\dot{\mathbf{P}}_p + \hat{\boldsymbol{\omega}}\mathbf{P}_p) \quad (18)$$

The following dynamic equations are obtained in the body frame:

$$\dot{\mathbf{P}} = \mathbf{P} \times \boldsymbol{\omega} + \mathbf{R}^T \sum_{i=1}^I \mathbf{f}_{ext,i} \quad (19)$$

$$\dot{\boldsymbol{\Pi}} = \boldsymbol{\Pi} \times \boldsymbol{\omega} + \mathbf{P} \times \mathbf{v} + \mathbf{R}^T \sum_{i=1}^I [(\mathbf{x}_i - \mathbf{b}) \times \mathbf{f}_{ext,i}] + \mathbf{R}^T \sum_{j=1}^J \boldsymbol{\tau}_{ext,j} \quad (20)$$

$$\dot{\mathbf{P}}_p = \mathbf{P}_p \times \boldsymbol{\omega} + m_p \mathbf{g} \mathbf{k} + \mathbf{R}^T \sum_{k=1}^K \mathbf{f}_{int,m_p} \quad (21)$$

Here, $\mathbf{R}^T \sum_{k=1}^K \mathbf{f}_{int,m_p}$ is the internal force exerted on the piston in the body-fixed frame. Let

$$\dot{\mathbf{P}}_p = \mathbf{u}_p = \mathbf{P}_p \times \boldsymbol{\omega} + m_p \mathbf{g} \mathbf{k} + \mathbf{R}^T \sum_{k=1}^K \mathbf{f}_{int,p} \quad (22)$$

The total kinetic energy of the glider fluid is calculated, and the kinetic energy of the piston and static mass is expressed as follows:

$$T_s = \frac{1}{2} (\mathbf{v})^T \begin{pmatrix} \mathbf{m}_s \mathbf{I}_{3 \times 3} & -\mathbf{m}_s \hat{\mathbf{r}}_s \\ \mathbf{m}_s \hat{\mathbf{r}}_s & \mathbf{J}_s \end{pmatrix} (\mathbf{v}) \quad (23)$$

$$T_p = \frac{1}{2} \begin{pmatrix} \mathbf{v} \\ \boldsymbol{\omega} \\ \dot{\mathbf{r}}_p \end{pmatrix}^T \begin{pmatrix} \mathbf{m}_p \mathbf{I}_{3 \times 3} & \mathbf{m}_p \hat{\mathbf{r}}_p & \mathbf{m}_p \mathbf{I}_{3 \times 3} \\ \mathbf{m}_p \hat{\mathbf{r}}_p & -\mathbf{m}_p \hat{\mathbf{r}}_p \hat{\mathbf{r}}_p & \mathbf{m}_p \hat{\mathbf{r}}_p \\ \mathbf{m}_p \mathbf{I}_{3 \times 3} & \mathbf{m}_p \hat{\mathbf{r}}_p & \mathbf{m}_p \mathbf{I}_{3 \times 3} \end{pmatrix} \begin{pmatrix} \mathbf{v} \\ \boldsymbol{\omega} \\ \dot{\mathbf{r}}_p \end{pmatrix} \quad (24)$$

The kinetic energy of a rigid body immersed in an ideal fluid can be expressed as follows:

$$T_f = \frac{1}{2} (\mathbf{v})^T \begin{pmatrix} \mathbf{M}_f & \mathbf{D}_f^T \\ \mathbf{D}_f & \mathbf{J}_f \end{pmatrix} (\mathbf{v}) \quad (25)$$

Here, \mathbf{M}_f is the added mass matrix, \mathbf{J}_f the added inertia matrix, and \mathbf{D}_f the added cross-term. These matrices are determined by the body shape and fluid density.

The total glider-fluid kinetic energy is expressed as:

$$T = T_s + T_p + T_f \quad (26)$$

Here, the inertia of the total system is expressed as:

$$\mathbf{I} = \begin{pmatrix} \mathbf{m}_s \mathbf{I}_{3 \times 3} + \mathbf{m}_p \mathbf{I}_{3 \times 3} + \mathbf{M}_f & -\mathbf{m}_p \hat{\mathbf{r}}_p + \mathbf{D}_f^T & \mathbf{m}_p \mathbf{I}_{3 \times 3} \\ \mathbf{m}_p \hat{\mathbf{r}}_p + \mathbf{D}_f & \mathbf{J}_s - \mathbf{m}_p \hat{\mathbf{r}}_p \hat{\mathbf{r}}_p + \mathbf{J}_f & \mathbf{m}_p \hat{\mathbf{r}}_p \\ \mathbf{m}_p \mathbf{I}_{3 \times 3} & -\mathbf{m}_p \hat{\mathbf{r}}_p & \mathbf{m}_p \mathbf{I}_{3 \times 3} \end{pmatrix} \quad (27)$$

\mathbf{P} , $\boldsymbol{\Pi}$, and \mathbf{P}_p can be calculated as follows:

$$\mathbf{P} = \frac{\partial T}{\partial \mathbf{v}} = (\mathbf{m}_s \mathbf{I}_{3 \times 3} + \mathbf{M}_f) \mathbf{v} + \mathbf{D}_f^T \boldsymbol{\omega} + m_p (\mathbf{v} + \boldsymbol{\omega} \times \mathbf{r}_p + \dot{\mathbf{r}}_p) \quad (28)$$

$$\boldsymbol{\Pi} = \frac{\partial T}{\partial \boldsymbol{\omega}} = \mathbf{D}_f \mathbf{v} + (\mathbf{J}_s + \mathbf{J}_f) \boldsymbol{\omega} + m_p \hat{\mathbf{r}}_p (\mathbf{v} + \boldsymbol{\omega} \times \mathbf{r}_p + \dot{\mathbf{r}}_p) \quad (29)$$

$$\mathbf{P}_p = m_p (\mathbf{v} + \boldsymbol{\omega} \times \mathbf{r}_p + \dot{\mathbf{r}}_p) \quad (30)$$

The design of this glider can be regarded as symmetric about three planes for calculation convenience, where \mathbf{M}_f and \mathbf{J}_f are diagonal matrices, and $\mathbf{D}_f = \mathbf{0}$. Let $\mathbf{M}_f = \text{diag}(m_{f1} \ m_{f2} \ m_{f3})$ and $\mathbf{J}_f = \text{diag}(J_{f1} \ J_{f2} \ J_{f3})$.

$$\mathbf{M} = \mathbf{m}_s \mathbf{I}_{3 \times 3} + \mathbf{M}_f = \begin{pmatrix} m_1 & 0 & 0 \\ 0 & m_2 & 0 \\ 0 & 0 & m_3 \end{pmatrix} \quad (31)$$

$$\mathbf{J} = \mathbf{J}_s + \mathbf{J}_f = \begin{pmatrix} J_1 & 0 & 0 \\ 0 & J_2 & 0 \\ 0 & 0 & J_3 \end{pmatrix} \quad (32)$$

The linear and angular momentum can be expressed as:

$$\begin{pmatrix} \mathbf{P} \\ \boldsymbol{\Pi} \\ \mathbf{P}_p \end{pmatrix} = \mathbf{I} \begin{pmatrix} \mathbf{v} \\ \boldsymbol{\omega} \\ \dot{\mathbf{r}}_p \end{pmatrix} \quad (33)$$

Here, the inertia matrix \mathbf{I} is expressed as:

$$\mathbf{I} = \begin{pmatrix} \mathbf{m}_p \mathbf{I}_{3 \times 3} + \mathbf{M} & -\mathbf{m}_p \hat{\mathbf{r}}_p & \mathbf{m}_p \mathbf{I}_{3 \times 3} \\ \mathbf{m}_p \hat{\mathbf{r}}_p & \mathbf{J} - \mathbf{m}_p \hat{\mathbf{r}}_p \hat{\mathbf{r}}_p & \mathbf{m}_p \hat{\mathbf{r}}_p \\ \mathbf{m}_p \mathbf{I}_{3 \times 3} & -\mathbf{m}_p \hat{\mathbf{r}}_p & \mathbf{m}_p \mathbf{I}_{3 \times 3} \end{pmatrix} \quad (34)$$

From Eq. (33), it is obtained

$$\begin{pmatrix} \mathbf{v} \\ \boldsymbol{\omega} \\ \dot{\mathbf{r}}_p \end{pmatrix} = \mathbf{I}^{-1} \begin{pmatrix} \mathbf{P} \\ \boldsymbol{\Pi} \\ \mathbf{P}_p \end{pmatrix} \quad (35)$$

The inverse of the inertia matrix is expressed as:

$$\mathbf{I}^{-1} = \begin{pmatrix} \mathbf{M}^{-1} & 0 & \mathbf{M}^{-1} \\ \mathbf{0} & \mathbf{J}^{-1} & -\mathbf{J}^{-1}\hat{\mathbf{r}}_p \\ \mathbf{M}^{-1} & \hat{\mathbf{r}}_p\mathbf{J}^{-1} & \mathbf{M}^{-1} - \hat{\mathbf{r}}_p\mathbf{J}^{-1}\hat{\mathbf{r}}_p + \frac{1}{m_p}\mathbf{I}_{3 \times 3} \end{pmatrix} \quad (36)$$

The position of the piston can be represented as:

$$\mathbf{r}_p = \mathbf{r}_{pi} + \mathbf{d}_p \quad (37)$$

\mathbf{r}_{pi} is the initial position of the piston, the position coordinates of the piston can also be expressed as:

$$\dot{\mathbf{r}}_p = \dot{\mathbf{d}}_p \quad (38)$$

Combining the equations above, the equations of motion governing an HTAUUV propagating in a three-dimensional space are expressed as follows:

$$\begin{pmatrix} \dot{\mathbf{R}} \\ \dot{\mathbf{b}} \\ \dot{\boldsymbol{\omega}} \\ \dot{\mathbf{v}} \\ \dot{\mathbf{r}}_p \\ \dot{\mathbf{P}}_p \\ \dot{\dot{\mathbf{P}}}_p \\ \dot{\mathbf{m}}_0 \end{pmatrix} = \begin{pmatrix} \mathbf{R}\hat{\boldsymbol{\omega}} \\ \mathbf{R}\mathbf{v} \\ \mathbf{J}^{-1}\boldsymbol{\tau} \\ \mathbf{M}^{-1}\mathbf{F} \\ \dot{\mathbf{d}}_p \\ m_p(\mathbf{v} + \boldsymbol{\omega} \times \mathbf{r}_p + \dot{\mathbf{r}}_p) \\ \mathbf{u}_p \\ 2u_0\dot{\mathbf{d}}_p \end{pmatrix} \quad (39)$$

The total moment and force are expressed as follows:

$$\boldsymbol{\tau} = (\mathbf{J}\boldsymbol{\omega} + \hat{\mathbf{r}}_p\mathbf{P}_p) \times \boldsymbol{\omega} + \mathbf{M}\mathbf{v} \times \mathbf{v} + \boldsymbol{\omega} \times \mathbf{r}_p \times \mathbf{P}_p + m_p\hat{\mathbf{r}}_p g \mathbf{R}^T \mathbf{k} + \boldsymbol{\tau}_{ext} - \hat{\mathbf{r}}_p \mathbf{u}_p \quad (40)$$

$$\mathbf{F} = (\mathbf{M}\mathbf{v} + \mathbf{P}_p) \times \boldsymbol{\omega} + m_0 g \mathbf{R}^T \mathbf{k} + \mathbf{F}_{ext} - \mathbf{u}_p \quad (41)$$

Here, $\boldsymbol{\tau}_{ext}$ and \mathbf{F}_{ext} are the hydrodynamic moment, lift, and drag forces exerted on the glider, respectively.

The purpose of this paper is to study pitch control for the HTAUUV using the elevator in the vertical plane. Therefore, the set of motion control equations in three-dimensional space has been simplified to the set of equations in the vertical plane [17].

$$\dot{x} = v_1 \cos\theta + v_3 \sin\theta \quad (42)$$

$$\dot{z} = -v_1 \sin\theta + v_3 \cos\theta \quad (43)$$

$$\dot{\theta} = \omega_2 \quad (44)$$

$$\dot{v}_1 = \frac{1}{m_1} [(-m_3 v_3 \omega_2 - P_{p3} \omega_2) - m_0 g \sin\theta + (L \sin\alpha - D \cos\alpha) - u_{p1}] \quad (45)$$

$$\dot{v}_3 = \frac{1}{m_3} [(-m_1 v_1 \omega_2 + P_{p1} \omega_2) + m_0 g \cos\theta - (L \cos\alpha + D \sin\alpha) - u_{p3}] \quad (46)$$

$$\dot{\omega}_2 = \frac{1}{J_2} \left[\begin{array}{c} (m_3 - m_1)v_1v_3 - (r_{p1}P_{p1} + r_{p3}P_{p3})\omega_2 \\ -mg(r_{rx} \cos \theta + r_{rz} \sin \theta) + M_{DL} - r_{p3}u_{p1} + r_{p1}u_{p3} \end{array} \right] \quad (47)$$

$$\dot{r}_{p1} = \dot{d}_{p1} \quad (48)$$

$$P_{p1} = m_p(v_1 + \omega_2 r_{p3} + \dot{d}_{p1}) \quad (49)$$

$$P_{p3} = m_p(v_3 - \omega_2 r_{p1}) \quad (50)$$

$$\dot{P}_{p1} = u_{p1} \quad (51)$$

$$\dot{P}_{p3} = u_{p3} \quad (52)$$

$$\dot{m}_0 = 2u_0\dot{d}_{p1} \quad (53)$$

$$\alpha = \arctan \frac{v_3}{v_1} \quad (54)$$

$$\zeta = \theta - \alpha \quad (55)$$

Here, x and z are the horizontal and vertical displacements of the HTAUV in the inertial frame, respectively; α is the angle of attack; θ is the pitching angle; ζ is the gliding angle; v_1 and v_3 are the velocity components of the HTAUV along the x-axes and z-axes in the body frame, respectively; r_{rx} and r_{rz} are the mass center of the HTAUV along the x-axes and z-axes in the body frame, respectively; ω_2 represents the pitch angular velocity of the HTAUV rotating about the y-axis of the body frame; L is the hydrodynamic lift; D is the hydrodynamic drag; M_{DL} represents the pitching moment yielded by the hydrodynamic analysis; m_1 and m_3 represent the added mass along the x-axes and z-axes, respectively; J_2 represents the moment of inertia rotating about the y-axis; P_{p1} and P_{p3} represent the momenta of piston along the x-axes and z-axes, respectively.

3. Hydrodynamic Analysis

The various hydrodynamic parameters of underwater equipment in operation are obtained very accurately through experiments. Due to the development of computer software technology, more and more researchers are utilizing computer software to simulate the actual experimental process. Compared to traditional experiments, computer simulation will be faster and cheaper to obtain simulation data that are more consistent with experimental results. In this paper, Ansys Fluent was used to simulate the hydrodynamic behavior of HTAUV.

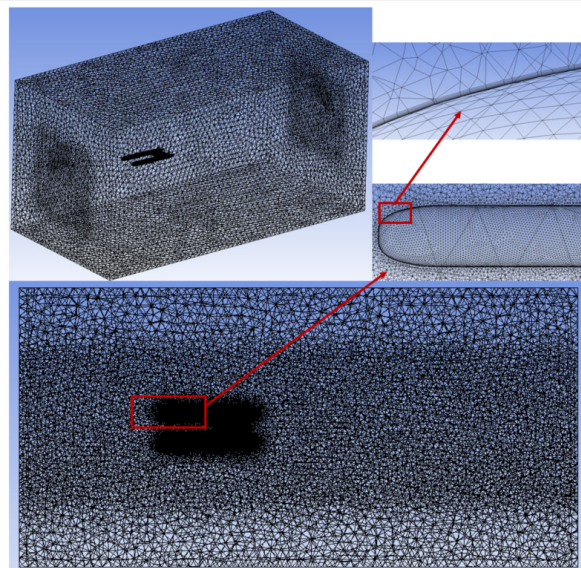


Fig. 6 Non-structural grid of CFD simulation [15]

The simulation domain is a rectangular body with dimensions of 14 m in length, and 6 m in both width and height, and the inlet of the simulation domain is 5 m away from the center of buoyancy of the HTAUV. The k-omega shear-stress-transport (SST) model is selected as the turbulence model for this simulation [18], as it is widely used for simulating underwater equipment. CFD is an efficient and fast simulation tool, which can complete a complex experimental process in the shortest time and with the least cost, greatly facilitating the progress of research. Simulation results can be used to understand the water flow around the HTAUV. Due to the complexity of the HTAUV structure, a non-structural grid is used for the CFD simulation in this paper, with a total grid number of about 3,790,000 and a Y-plus of less than 1. The CFD simulation conditions are as follows: the entrance velocity is from 0.25 m/s to 1.5 m/s with a velocity interval of 0.25 m/s; the angle of attack is from -12 degrees to +12 degrees with an angular interval of 2 degrees; and the deflection angle of the elevator is from -16 degrees to +16 degrees with a deflection angle interval of 2 degrees. The created grid is shown in Fig.6.

Fig. 7 and Fig. 8 show the current velocity contours of the elevator at different deflection angles during the upward and downward dives, respectively. Since the HTAUV is an approximately symmetric structure about the xz plane, an isosurface is created at the xz plane in the Ansys Fluent post-processing to observe the behavior of the fluid in the vicinity of the elevator. The elevator is marked by a red circle in the figures, with a positive deflection angle corresponding to downward deflection and a negative deflection angle corresponding to upward deflection.

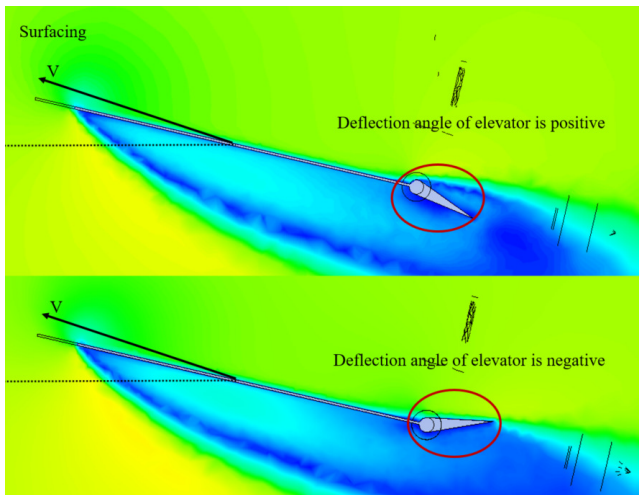


Fig. 7 Velocity contour during surfacing

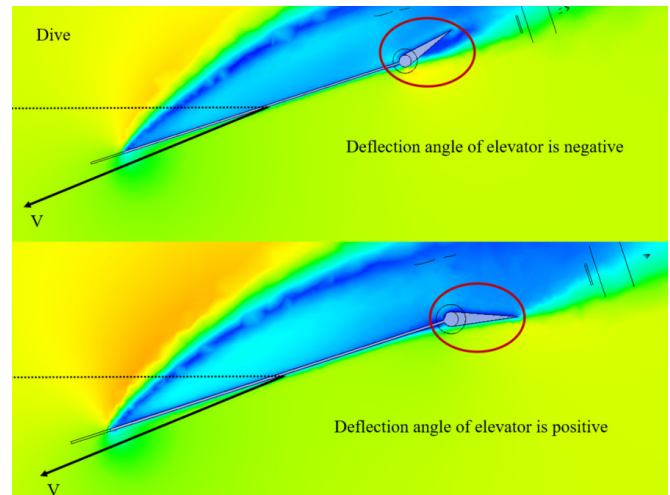


Fig. 8 Velocity contour during dive

Based on the above two figures, it can be concluded that during the surfacing process, if the elevator deflection angle is positive, the current wake caused by the fixed airfoil will affect the elevator, leading to unstable simulation data. Similarly, during a dive, a negative deflection angle of the elevator will also cause disturbance from the current wake, resulting in unstable simulation results. To achieve a stable glide of the HTAUV underwater, it is recommended to set a positive deflection angle of the elevator during a dive and a negative deflection angle during surfacing. Fig. 9 illustrates the fluid velocity contours in the vicinity of the HTAUV body at an angle of attack of 2 degrees and a velocity of 0.5 m/s.

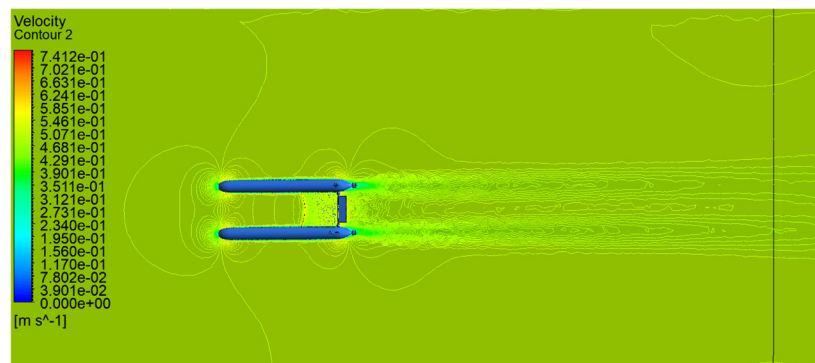


Fig. 9 Velocity contour around HTAUV

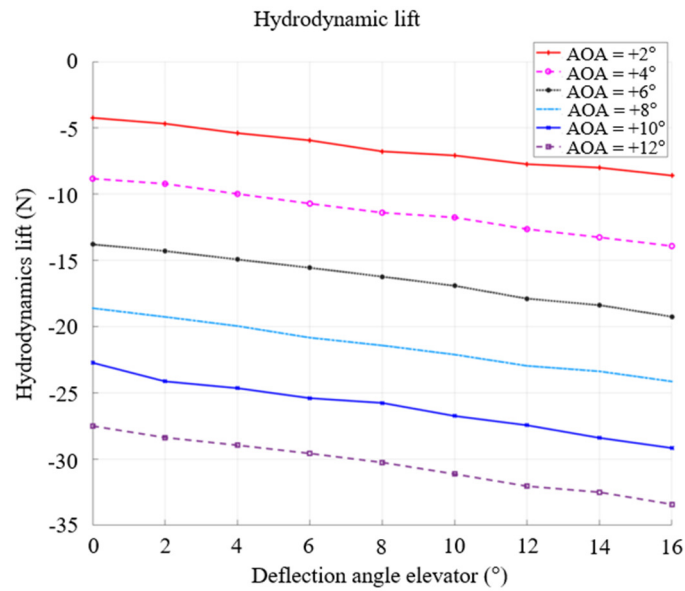


Fig. 10 Relationship between hydrodynamic lift and elevator deflection angle

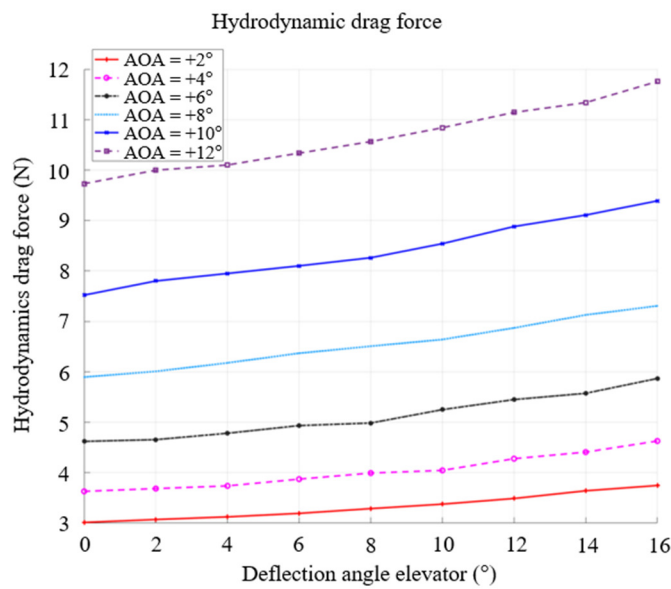


Fig. 11 Relationship between hydrodynamic drag and elevator deflection angle

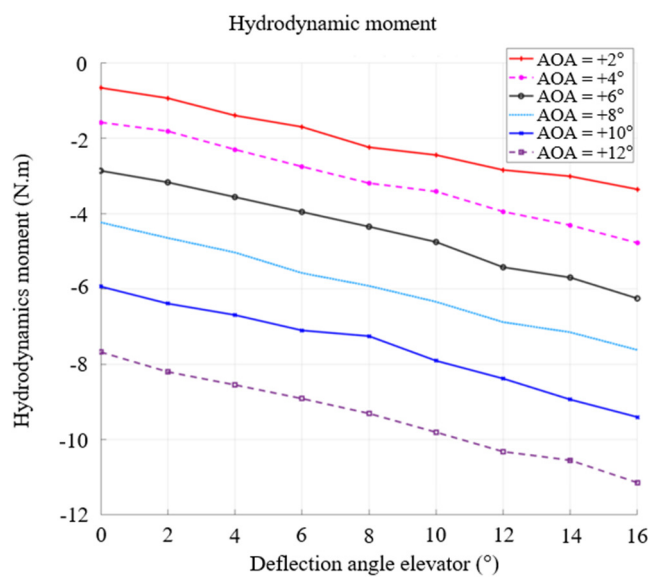


Fig. 12 Relationship between hydrodynamic moment and elevator deflection angle

To determine the relationship between hydrodynamic parameters and elevator angle, Ansys Fluent was used to simulate and gather hydrodynamic data, including hydrodynamic lift, hydrodynamic drag, and hydrodynamic moment. In this paper, the least squares method is used to fit the simulation data. Firstly, the relationship between hydrodynamic coefficients and angle of attack and velocity is derived by assuming that the deflection angle of the elevator is 0. Then, the relationship between hydrodynamic forces and the deflection angle of the elevator is fitted for a fixed velocity and angle of attack. Figs. 10-12 depict statistical graphs of the hydrodynamic data under different elevator deflection angles, with a simulation glide speed of 0.5 m/s.

Based on the hydrodynamic relationship diagram, it can be concluded that when the angle of attack and velocity are fixed, the absolute values of hydrodynamic lift, drag, and the moment all increase in an approximately linearly proportional manner as the elevator deflection angle increases. Therefore, the relationship between hydrodynamic force and elevator deflection angle can be expressed using the following equation:

$$L = (K_{L0} + K_L \alpha) V^2 + K_{L\delta} \delta V^2 \quad (56)$$

$$D = (K_{D0} + K_D \alpha^2) V^2 + K_{D\delta} \delta V^2 \quad (57)$$

$$M_{DL} = (K_{M0} + K_M \alpha) V^2 + K_{M\delta} \delta V^2 \quad (58)$$

Here, K_{L0} and K_L are hydrodynamic lift parameters, with K_{L0} representing the parameter at an angle of attack of 0; $K_{L\delta}$ is the hydrodynamic lift parameter associated with the angle of deflection of the elevator; δ represents the deflection angle of the elevator. Similarly, K_{D0} and K_D are hydrodynamic drag parameters, and $K_{D\delta}$ is the hydrodynamic drag parameter associated with the angle of deflection of the elevator. K_{M0} and K_M are hydrodynamic moment parameters, and $K_{M\delta}$ is the hydrodynamic moment parameter associated with the angle of deflection of the elevator. Since the HTAUUV is approximately symmetric in structure about the xz plane, the hydrodynamic changes caused by the elevator deflection angle during upward and downward dives can be considered approximately equal.

4. Simulation Results

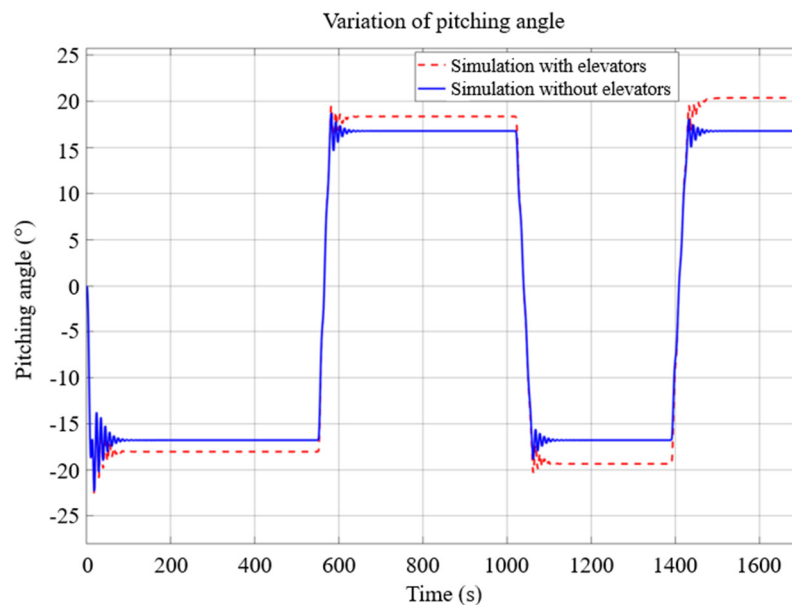


Fig. 13 Comparison of pitching angle

The equations of motion for the HTAUUV and the corresponding hydrodynamic expressions caused by the angle of deflection of the elevator have been obtained. Matlab/Simulink was used to simulate the motion of the HTAUUV concerning the displacement of the piston in the buoyancy engine and the deflection angle of the elevator. When the piston absorbs water, the buoyancy of the HTAUUV decreases, leading it to sink as gravity is larger than the buoyancy. However, under the influence

of the hydrodynamic force generated by the fixed wing, the HTAUV begins to glide forward. The gliding attitude of the HTAUV underwater can be adjusted by controlling the downward deflection angle of the elevator. Figs. 13-15 depict a comparison of simulation data for the HTAUV with and without elevators under the same net buoyancy conditions.

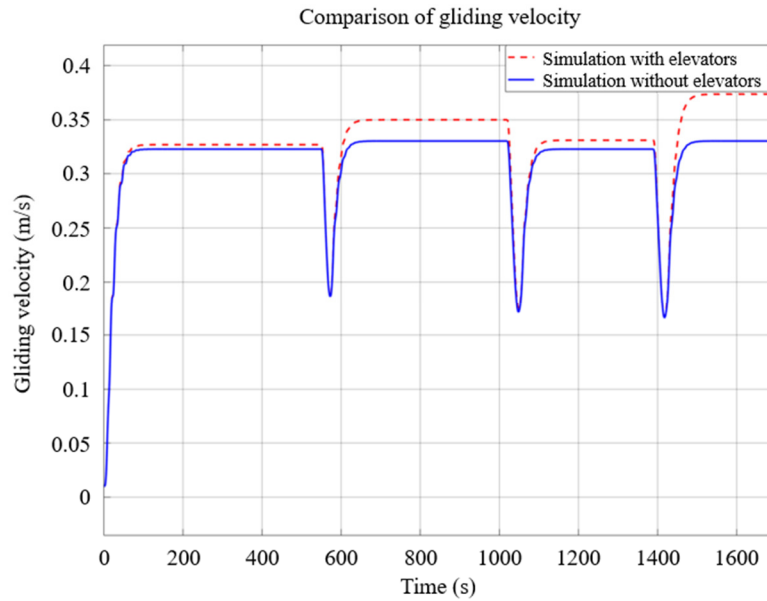


Fig. 14 Comparison of gliding velocity

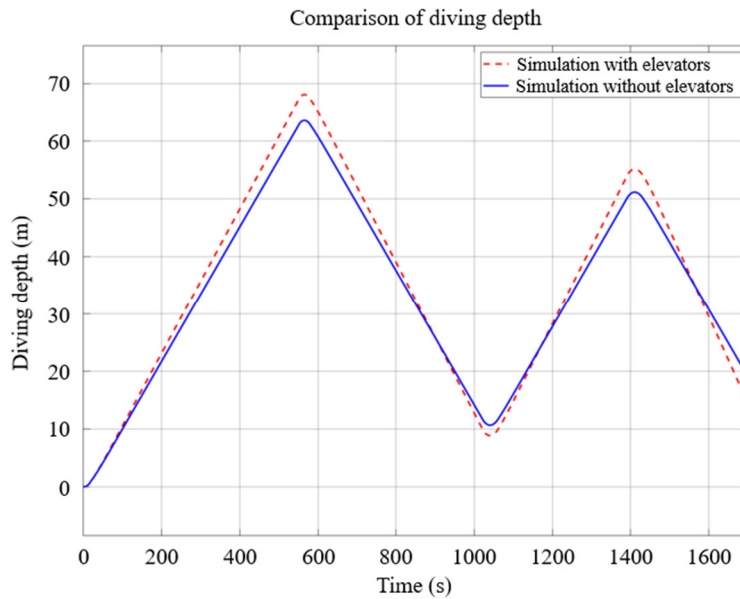


Fig. 15 Comparison of diving depth

Fig. 13 shows the simulation curves for pitch angle under two different conditions. Fig. 14 and Fig. 15 present the comparison curves for the glide speed and dive depth, respectively. It is clear from the comparisons in Figs. 13 to 15 that the simulation results with elevators involved are greater than those without elevators. In the case of equal net buoyancy, the glide speed, pitch angle, and dive depth of HTAUV after the positive deflection of the elevator angle during the dive are larger than the values of the elevator without deflection. The same result can be found when the elevator undergoes a negative deflection during the surfacing process, i.e., the glide parameter with the elevator is larger than the value without the elevator.

5. Conclusions

This paper presents a new design for an HTAUV that consists of dual-cylinder hulls and analyzes its pitching motion using elevators and a buoyancy engine. Specifically, the study focuses on the motion of the HTAUV that is influenced by the

deflection angle of the elevators. To investigate this relationship, the hydrodynamic parameters of the HTAUV and the deflection angle of the elevators were studied through CFD simulations. The hydrodynamic parameters of HTAUV including hydrodynamic lift, drag, and hydrodynamic moment are obtained through CFD simulation. The post-processing operation of the simulation results in Ansys Fluent enabling easy observation of the fluid behavior in the vicinity of the HTAUV and elevator.

In MATLAB, the hydrodynamic data were fitted to obtain the relationship between variations in hydrodynamic forces and the deflection angle of the elevator, considering a given angle of attack and velocity. This process resulted in deriving mathematical equations for the hydrodynamic forces concerning the velocity, angle of attack, and deflection angle of the elevator. In the motion simulation of the HTAUV, when the elevator is deflected, the resulting glide velocity, glide angle, and pitch angle of the HTAUV are larger compared to the results obtained when the elevator is not deflected, all under the same net buoyancy condition. In this paper, the relationship between the pitch attitude of the HTAUV in the vertical plane and the elevator deflection angle is considered, and the accuracy of the simulation results in this paper will be verified utilizing experiments in the future.

Conflicts of Interest

The authors declare no conflict of interest.

Acknowledgment

This work was supported by the development of an unmanned remote construction-aided system for a harbor infrastructure project, funded by the Ministry of Oceans and Fisheries, Korea. References and development of biomimetic underwater undulating robot funded by the Agency of Defense Development.

Reference

- [1] P. V. Patil, M. K. Khan, M. Korulla, V. Nagarajan, and O. P. Sha, "Design Optimization of an AUV for Performing Depth Control Maneuver," *Ocean Engineering*, vol. 266, part 5, article no. 112929, December 2022.
- [2] A. Hammoud, J. Sahili, M. Madi, and E. Maalouf, "Design and Dynamic Modeling of ROVs: Estimating the Damping and Added Mass Parameters," *Ocean Engineering*, vol. 239, article no. 109818, November 2021
- [3] C. Cheng, Q. Sha, B. He, and G. Li, "Path Planning and Obstacle Avoidance for AUV: A Review," *Ocean Engineering*, vol. 235, article no. 109355, September 2021.
- [4] H. Wu, W. Niu, S. Wang, and S. Yan, "An Optimization Method for Control Parameters of Underwater Gliders considering Energy Consumption and Motion Accuracy," *Applied Mathematical Modelling*, vol. 90, pp. 1099-1119, February 2021
- [5] M. Q. He, C. D. Williams, P. Crocker, D. Shea, N. Riggs, and R. Bachmayer, "A Simulator Developed for a Twin-Pod AUV, the Marport SQX-500," *Journal of Hydrodynamics, Ser. B*, vol. 22, no. 5, supplement 1, pp. 184-189, October 2010.
- [6] P. J. B. Sánchez, M. Papaelias, and F. P. G. Márquez, "Autonomous Underwater Vehicles: Instrumentation and Measurements," *IEEE Instrumentation & Measurement Magazine*, vol. 23, no. 2, pp. 105-114, April 2020.
- [7] D. Li and L. Du, "AUV Trajectory Tracking Models and Control Strategies: A Review," *Journal of Marine Science and Engineering*, vol. 9, no. 9, article no. 1020, September 2021.
- [8] C. G. D. Bono and L. G. Buttarò, "Drag Based Shape Optimization of Submarines and AUVs Using CFD Analysis," unpublished.
- [9] J. Huang, H. S. Choi, M. T. Vu, D. W. Jung, K. B. Choo, H. J. Cho, et al., "Study on Position and Shape Effect of the Wings on Motion of Underwater Gliders," *Journal of Marine Science and Engineering*, vol. 10, no. 7, article no. 891, July 2022.
- [10] K. Stryczniewicz and P. Drężek, "CFD Approach to Modelling Hydrodynamic Characteristics of Underwater Glider," *Transactions on Aerospace Research*, vol. 4, no. 257, pp. 32-45, 2019.

- [11] T. L. Le, T. H. Vuong, and T. N. Tran, "A Computational Fluid Dynamics Study on the Design Optimization of an Autonomous Underwater Vehicle," *VNUHCM Journal of Science and Technology Development*, vol. 24, no. 2, pp. 1962-1966, May 2021.
- [12] T. L. Le and D. T. Hong, "Computational Fluid Dynamics Study of the Hydrodynamic Characteristics of a Torpedo-Shaped Underwater Glider," *Fluids*, vol. 6, no. 7, article no. 252, July 2021.
- [13] N. D. Nguyen, H. S. Choi, H. S. Jin, J. Huang, and J. H. Lee, "Robust Adaptive Depth Control of Hybrid Underwater Glider in Vertical Plane," *Advances in Technology Innovation*, vol. 5, no. 3, pp. 135-146, July 2020.
- [14] T. Q. M. Nhat, H. S. Choi, M. T. Vu, J. Sur, J. I. Kang, and H. J. Son, "On the Position Determination of Docking Station for AUVs Using Optical Sensor and Neural Network," *International Journal of Engineering and Technology Innovation*, vol. 10, no. 1, pp. 15-24, January 2020.
- [15] J. Huang, H. S. Choi, D. W. Jung, J. H. Lee, M. J. Kim, K. B. Choo, et al., "Design and Motion Simulation of an Underwater Glider in the Vertical Plane," *Applied Sciences*, vol. 11, no. 17, article no. 8212, September 2021.
- [16] J. G. Graver, "Underwater Gliders: Dynamics, Control and Design," Ph.D. dissertation, Department of Mechanical and Aerospace Engineering, Princeton University, Princeton, NJ, 2005.
- [17] J. Huang, H. S. Choi, D. W. Jung, K. B. Choo, H. Cho, P. H. N. Anh, et al., "Analysis of a New Twin Hybrid Autonomous Underwater Vehicle," *Applied Sciences*, vol. 13, no. 3, article no. 1551, February 2023.
- [18] Y. Singh, S. K. Bhattacharyya, and V. G. Idichandy, "CFD Approach to Steady State Analysis of an Underwater Glider," *2014 Oceans - St. John's*, pp. 1-5, September 2014.



Copyright© by the authors. Licensee TAETI, Taiwan. This article is an open-access article distributed under the terms and conditions of the Creative Commons Attribution (CC BY-NC) license (<https://creativecommons.org/licenses/by-nc/4.0/>).